Awatef A. Hamed

Widen Tabakoff

Department of Aerospace Engineering and Engineering Mechanics, University of Cincinnati, Cincinnati, OH 45220

Richard B. Rivir

Aeropropulsion and Power Directorate, Air Force Research Laboratory, Wright Laboratories Building 18, Wright Patterson AFB, OH 45433

Kaushik Das

Puneet Arora

Department of Aerospace Engineering and Engineering Mechanics, University of Cincinnati, Cincinnati, OH 45220

Turbine Blade Surface Deterioration by Erosion

This paper presents the results of a combined experimental and computational research program to investigate turbine vane and blade material surface deterioration caused by solid particle impacts. Tests are conducted in the erosion wind tunnel for coated and uncoated blade materials at various impact conditions. Surface roughness measurements obtained prior and subsequent to the erosion tests are used to characterize the change in roughness caused by erosion. Numerical simulations for the three-dimensional flow field and particle trajectories through a low-pressure gas turbine are employed to determine the particle impact conditions with stator vanes and rotor blades using experimentally based particle restitution models. Experimental results are presented for the measured blade material/coating erosion and surface roughness. The measurements indicate that both erosion and surface roughness increase with impact angle and particle size. Computational results are presented for the particle trajectories through the first stage of a low-pressure turbine of a high bypass turbofan engine. The trajectories indicate that the particles impact the vane pressure surface and the aft part of the suction surface. The impacts reduce the particle momentum through the stator but increase it through the rotor. Vane and blade surface erosion patterns are predicted based on the computed trajectories and the experimentally measured blade coating erosion characteristics. [DOI: 10.1115/1.1860376]

Introduction

Gas turbine materials have progressed rapidly beyond traditional ferrous alloys. New blade coatings and materials are continuously being developed to meet the challenging requirements of modern gas turbine engines. Because of the serious consequences of erosion on gas turbine life and performance, it is necessary to gain a better understanding of the blade surface degradation mechanisms. A complex phenomenon, such as blade surface deterioration by erosion, requires a combination of experimental and computational research efforts [1]. Experimental studies require special high-temperature erosion wind tunnels to simulate the wide range of aerodynamic and thermal conditions in modern gas turbines. Erosion test results for gas turbine super alloys and coatings demonstrated that the eroding particle characteristics are affected by temperature and impact conditions [2–4].

In compressors, erosion by particle impacts reduces the blade chord, alters the shape of the leading and trailing edges, and increases the blade surface roughness [5,6]. Surface roughness measurements on gas turbine blades indicated an order-of-magnitude increase in rms roughness [7,8]. Bons et al. [9] conducted surface roughness measurements on in-service blades and vanes of ground-based turbines. They concluded that the operating conditions and service history determine the resulting blade erosion and roughness, and documented, on average, roughness levels 4–8 times greater than the levels for production hardware. Several investigators [10–13] reported increased heat transfer on turbine blades with simulated roughness.

Particle size affects the blade impact patterns because smaller particles tend to follow the flow while larger particles impact the vane and rotor blades. However, even particles of 1–30 μm have been known to damage exposed components of coal-burning turbines [14]. Numerical simulations of the particle trajectories through gas turbine engines provide valuable information on the vane and blade impact patterns [1,15–18]. Accurate predictions require correlations based on reliable measurements of particle restitution characteristics in tunnels equipped with optical access [19,20].

In the current work, a combined experimental and numerical investigation was conducted to study the dynamics of suspended solid particles in gas turbine flows and the associated blade surface material degradation from particle surface impacts. The experimental studies characterize blade and coating material erosion and surface roughness variation with particle impact conditions. The numerical simulations of particle trajectories model the effects of aerodynamic forces on the particles through the three-dimensional (3D) turbine flow field, the change in the magnitude and direction of particle velocities due to impacts with the stationary and rotating turbine blade surfaces. The trajectory simulations provide the vane and blade surface impact patterns at the operating conditions associated with particle ingestion into the turbine. Predictions of vane and blade surface erosion patterns and the associated surface roughness are based on the computed particle impact statistics and the experimentally measured data.

Experimental Work

Tests were conducted to characterize the blade and coating material deterioration in terms of mass removal and change in surface roughness associated with particle impacts. The experiments were conducted over a range of impact angles corresponding to those encountered in the gas turbine environment. The tested samples were evaluated before and after they were tested in the tunnel with a calibrated mass of erosive particles to determine the eroded weight and to detect the change in surface roughness.

The University of Cincinnati (UC) erosion wind tunnel facility is shown schematically in Fig. 1. It consists of the following components: particle feeder (A), main air supply pipe (B), combustor (C), particle preheater (D), particle injector (E), acceleration tunnel (F), test section (G), and exhaust tank (H). Abrasive particles of a given constituency and measured weight are placed into the

Contributed by the International Gas Turbine Institute (IGTI) of THE AMERICAN SOCIETY OF MECHANICAL ENGINEERS for publication in the ASME JOURNAL OF TURBOMACHINERY. Paper presented at the International Gas Turbine and Aeroengine Congress and Exhibition, Vienna, Austria, June 13–17, 2004, Paper No. 2004-GT-54328. Manuscript received by IGTI, October 1, 2003; final revision, March 1, 2004. IGTI Review Chair: A. J. Strazisar.

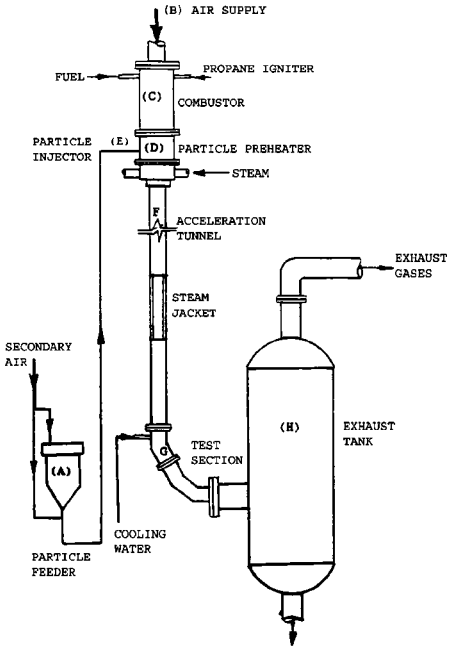

Fig. 1 Schematic of erosion test facility

particle feeder (A). The particles are fed into a secondary air source and blown into the particle preheater (D), and then to the injector (E), where they mix with the primary air supply (B), which is heated by the combustor (C). The particles are then accelerated via high velocity air in a constant-area steam-cooled duct (F) and impact the specimen in the test section (G). The particulate flow is then mixed with coolant and directed to the exhaust tank.

Varying the tunnel airflow controls particle velocity, while the particle impingement angle is controlled through the target sample rotation relative to the airflow. Heating the flow stream, which, in turn, heats the erosive media and sample(s), varies the temperature. As can be seen from Fig. 1, the tunnel geometry is uninterrupted from the acceleration tunnel throughout the test section in order to preserve the aerodynamics of the flow passing over the sample(s).

The tests were carried out for coupons of coated and uncoated power generation turbine blade materials. The coupons were mounted on a sample holder and placed in the erosion wind tunnel at the designated angles and subjected to erosion by a calibrated mass of particles. The holder protected all but one target coupon surface that was exposed to particle impacts. The samples were weighed, and their surface roughness was measured using a Taylor Hobson Talysurf before and after the erosion tests. Post erosion surface traverses were centered on the eroded portion of the sample. The two-dimensional (2D) surface roughness measurements of the coupon surface were sampled in two perpendicular directions. The arithmetic mean R_a, the root mean square deviation R_q, the maximum peak above the mean of the sample area R_p, and the maximum peak-to-valley dimension R_t of the roughness profile were determined from the unfiltered data. Three-dimensional measurements were taken in square millimeter areas at the center of selected samples to determine S_a, S_q, S_p, and S_t.

Computational Work

Numerical simulations were conducted to determine the three-dimensional flow field and the associated solid particle trajectories through a turbine stage. The compressible viscous flow and dispersed particle dynamics simulations were conducted using FLUENT 6.1 [21]. The gas phase simulations are based on the implicit solution of the Reynolds-averaged Navier-Stokes equations in conservation and the renormalization group (RNG) k-ε turbulence model with wall function [22]. The Lagrangian particle dynamics simulations were performed in the relative reference frame of each blade row and included models for the momentum exchanges with the flow field and blade passage surfaces.

Table 1 Particle size distribution

Particle size (μm)	% by weight finer than
1000	100
500	85–90
250	70–75
125	50–55
75	25–30
<75	10–15

Since the high inertia particle trajectories deviate from the flow and they impact the vane and blade surfaces. The simulations incorporate empirical particle-gas and particle-surface interaction models. Particle-gas interaction models represent the momentum exchange between the two phases through the aerodynamic forces due to the motion of particles relative to the gas flow field. Particle-surface interaction models in the trajectory simulations are based on correlations of laser Doppler velocimetry (LDV)-measured particle restitution characteristics [23,24].

Particle trajectories are determined from the stepwise integration of their equations of motion in each blade row reference frame

$$\frac{d\bar{u}_p}{dt} = F_D(\bar{u} - \bar{u}_p) + \frac{\bar{g}(\rho_p - \rho)}{\rho_p} + \bar{F}_R$$

The terms on the right-hand side represent the aerodynamic, gravitational, and forces acting on the particle due to the reference frame rotation. Neglecting interparticle collisions and particle rotation drag is the main aerodynamic force on high inertia particles

$$F_D = \frac{18\ \mu}{\rho_p D_p^2}\frac{C_D \mathrm{Re}}{24}$$

The following expression was used for the drag coefficient [25]:

$$C_D = \frac{24(1 + b_1 \mathrm{Re}^{b_2})}{\mathrm{Re}} + \frac{b_3 \mathrm{Re}}{b_4 + \mathrm{Re}}$$

The Reynolds number Re is based on the slip velocity and particle diameter, and the coefficients b_1, b_2, b_3, and b_4 are functions of the particle shape factor [21].

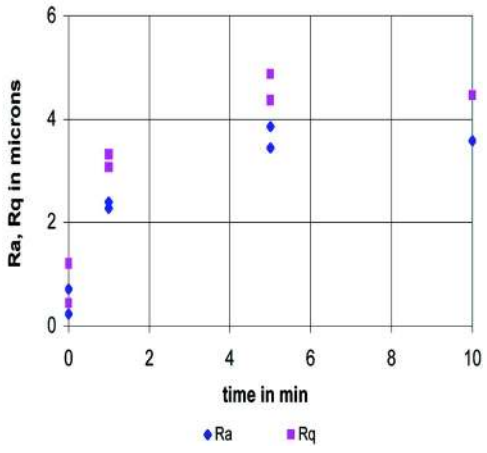

Fig. 2 Measured surface roughness for coated samples in erosion tests with 1500 μm crushed quartz at 90 deg

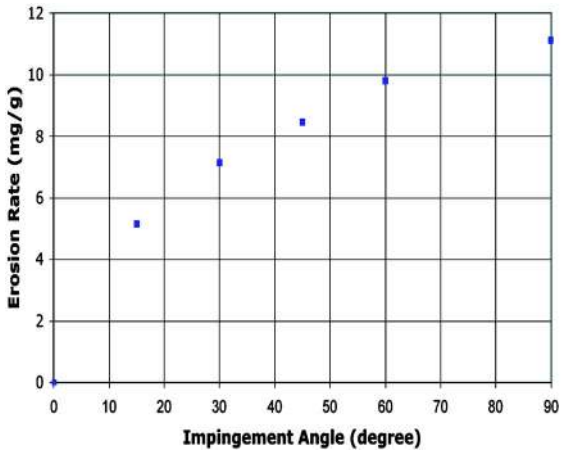

Fig. 3 Change in erosion rate with impingement angle for 1500 μm crushed quartz at 600 ft/s

The force $\bar{F}_R$ due to reference frame rotation is zero in the stator, but includes the centrifugal force and Coriolis acceleration in the rotor.

Results and Discussions

Erosion tests were conducted with runway sand and 1500 μm crushed quartz particles at 300 and 600 ft/s. The size distribution for runway sand is given in Table 1; its composition is 60% quartz, 26% gypsum, 12% calcite, and 2% soluble salts. Test coupons measuring 3×2 cm were cut from bars of coated and uncoated ground-based turbine blade materials. Before sectioning, the bar was traversed at 2.54 cm intervals along the centerline. Typical pre-erosion values of surface roughness were 1.07–2.14 μm for R_a, 1.12–4.08 μm for R_q, and 8.44–26.14 μm for R_t. Two- and three-dimensional traverses were performed on the target face after the erosion tests. The 2D traverses were 5–10 mm in length and were taken in two orthogonal directions with a minimum of 1000 points per traverse. The 3D traverses were 3×3 mm to 5×5 mm with a minimum of 1,000,000 points.

A set of erosion tests was performed initially in order to establish the erosive particle mass required to affect surface roughness in subsequent accelerated erosion tests. The results of these tests are presented in Fig. 2 for 1500 μm crushed quartz particles at 600 ft/s. The figure indicates negligible change in the surface roughness between the 5 and 10 min erosion tests. Experimental results from accelerated erosion tests of coated coupons are presented in Fig. 3 for quartz particles at 600 ft/s and Fig. 4 for runway sand at 300 ft/s. These results show that the erosion rate increases with increased velocity and impingement angle and that it is much higher in the case of 1500 μm crushed quartz. The corresponding change in measured roughness parameters with particle impact angle is shown in Fig. 5 for targets eroded by runway sand at 300 ft/s.

A photograph (magnification 2.8×) of an eroded coupon sample is shown in Fig. 6. One can see the contrast between the eroded and the uneroded portion on the right-hand side where the sample was covered by the clamp. The pictured surface measured

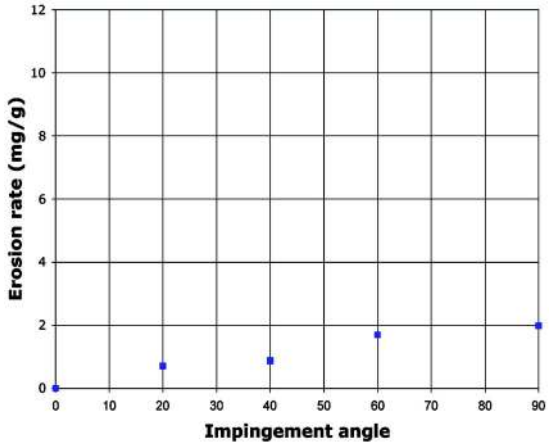

Fig. 4 Change in erosion rate with impingement angle for runway sand at 300 ft/s

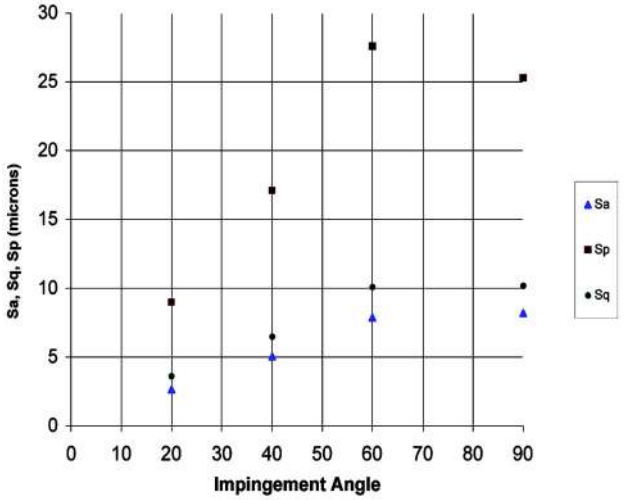

Fig. 5 Effect of impingement angle on eroded surface roughness for runway sand at 300 ft/s

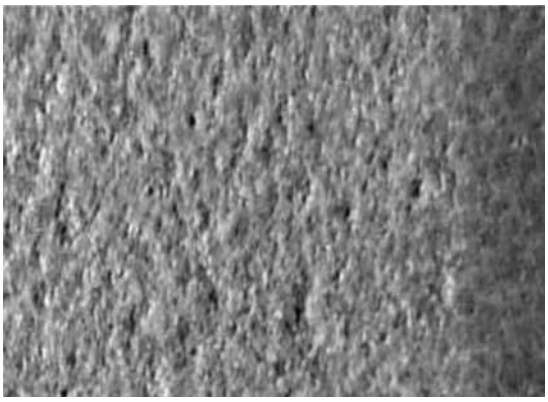

Fig. 6 Coated sample surface after testing at 300 ft/s with runway sand at 60 deg impingement angle

Table 2 Roughness parameters for pressure surface roughened blade

Location	R_a	R_q	R_p	R_t
Suction side, leading edge	5.75	7.30	13.82	44.10
Pressure side, leading edge	3.93	5.72	11.84	36.37
Pressure side, midchord	3.28	4.51	9.63	31.92
Pressure side, trailing edge	4.04	5.16	12.60	33.24

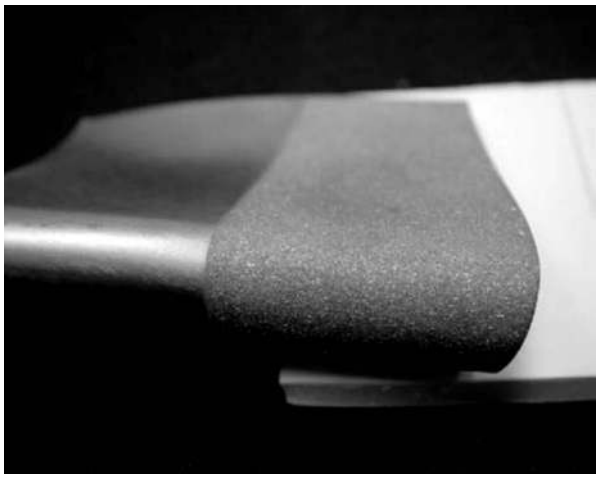

Fig. 7 Vane subjected to 1500 μm particles, 300 ft/s, 30 deg incidence. Erosion rate 5 mg/g of particles.

R_a=3.58 μm along the major axis and 3.34 μm along the minor axis compared to R_a=0.2736 μm in the clamped area.

AFRL provided a stainless steel vane with R_a surface finish of 0.34 μm for erosion testing. Table 2 summarizes the measured vane surface roughness after being subjected to impact with 20 g of 1500 μm crushed quartz particles at 300 ft/s and 30 deg angle of attack for 17 min. The measurements were obtained from four spanwise traverses. Traverse 1 was on the suction side of the leading edge and traverses 2–4 were equally spaced on the eroded pressure surface. Figure 7 presents a photograph of the eroded vane surface.

Table 3 Geometrical parameters for GE E^3 LP Turbine

	Stator (in.)	Rotor (in.)
Blade height	3.35	4.13
Midspan chord	2.10	1.16
Midspan pitch	1.10	0.68

Numerical simulations were performed for the GE E^3 first stage LP turbine at inlet stagnation temperature and pressure of 2001.6 °Rankine and 36.94 psia, respectively. Table 3 lists the geometrical parameters for the stator vanes and rotor blades. A three-dimensional H-type grid was used for the stator and rotor. The computational grid consisted of 80 grid points in the streamwise direction, 50 grid points blade to blade, and 80 grid points in the spanwise direction. A highly stretched mesh spacing was employed in the regions close to the blade passage surfaces, with y^+=25, for the first point next to the wall.

The stagnation pressure and temperature were specified at the inlet with no-slip conditions at the stationary walls and prescribed velocity conditions at the rotating walls. At the exit boundary, the static pressure was specified at the hub, and the radial pressure distribution was determined from integrating the axisymmetric radial momentum equation. The particles were introduced after the flow solution was converged, based on a four-order-of-magnitude reduction in the residuals. Because the particle loadings encountered in gas turbine applications are sufficiently low, the solid

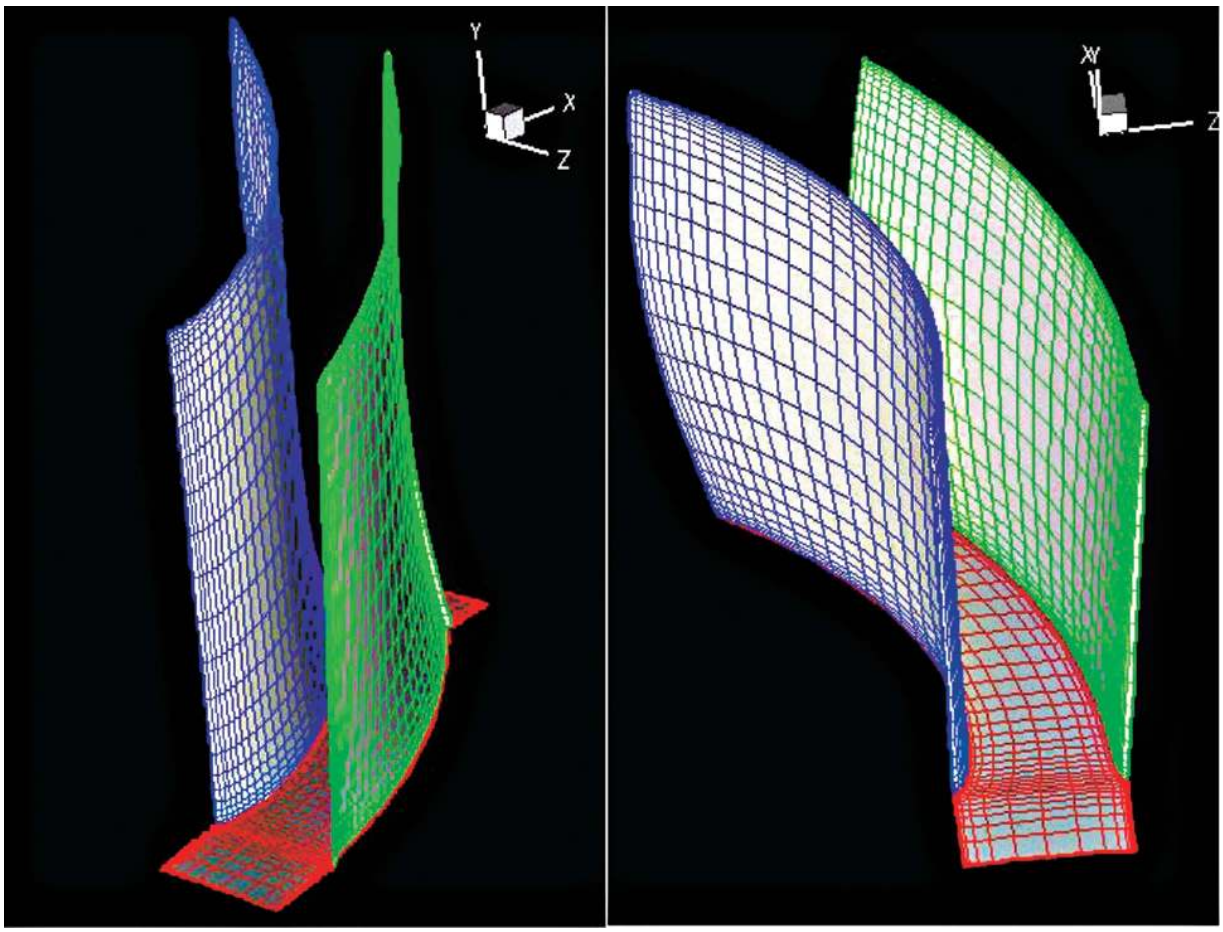

Fig. 8 Computational grid

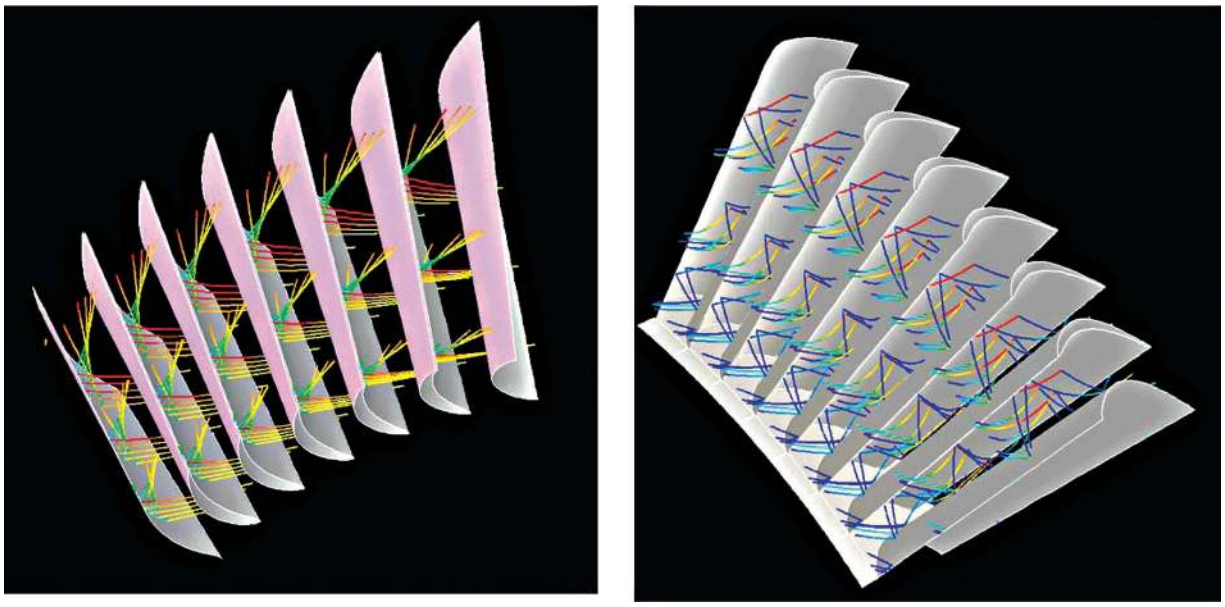

Fig. 9 30 μm particle trajectories: (a) (left) rear view of the stator and (b) (right) front view of the rotor

particle dynamics were simulated using one-way gas-particle interaction models, which do not take into consideration the effects of dispersed particles' momentum exchange on the gas flow field.

Figure 8 presents the grid used in the flow field, particle trajectories, and blade erosion rate computations. Figures 9–11 present the results of the 3D trajectory simulations for 30 and 1500 μm particles. Figure 9 shows that the 30 μm particles impact the vane pressure surface and that the vane impacts lower the particles' absolute velocities. This leads to a significant difference between the relative direction of particles as they enter the following rotor compared to the gas. The particles subsequently impact the rotor blade suction surface, as seen in Fig. 9(*b*). Figures 10 and 11 present the 30 and 1500 μm trajectories through the turbine stage mean diameter. The figures show that the inertia-dominated large particles cross the stator passage after impacting the vane pressure surface to impact the vane suction surface near the trailing edge. The smaller particles, on the other hand, also impact the vane pressure surface, but they are subsequently influenced by the gas flow and leave the flow passage without impacting the vane suction surface. The smaller particles enter the rotor blade passage and continue their trajectory after impacting the rotor blade suction surface. On the other hand, the large particles rebound from the rotor blades' leading edge and reenter the stator. In general, the particles centrifuge in the radial direction after the vane and blade surface impacts. In general, the large particles encounter more vane and blade surface impacts than the smaller particles.

The experimentally measured blade material erosion data together with the vane surface impact data from 2000 particle trajectory simulations were used to compute the vane surface erosion. Figure 12 presents the vane surface impact frequency distribution (the number of impacts per unit area per gram of ingested particles in the turbine). Figure 13 presents the corresponding impingement angles' mean values. The experimentally measured erosion rate of Fig. 4 was then used along with the vane

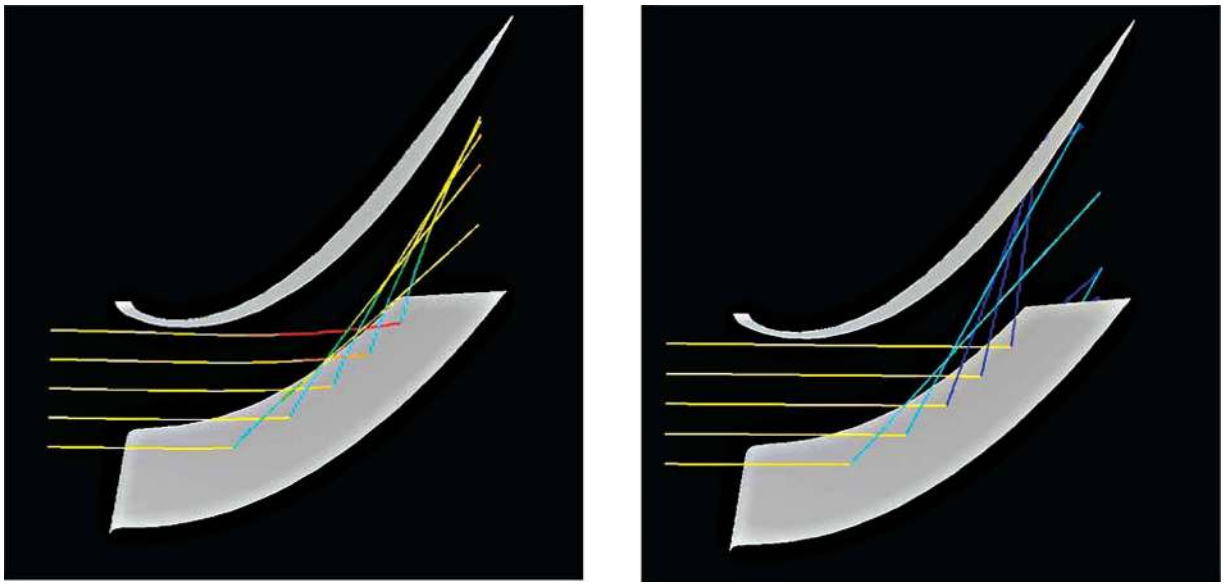

Fig. 10 Top view of particle trajectories through stator: (a) (left) 30 μm particles and (b) (right) 1500 μm particles

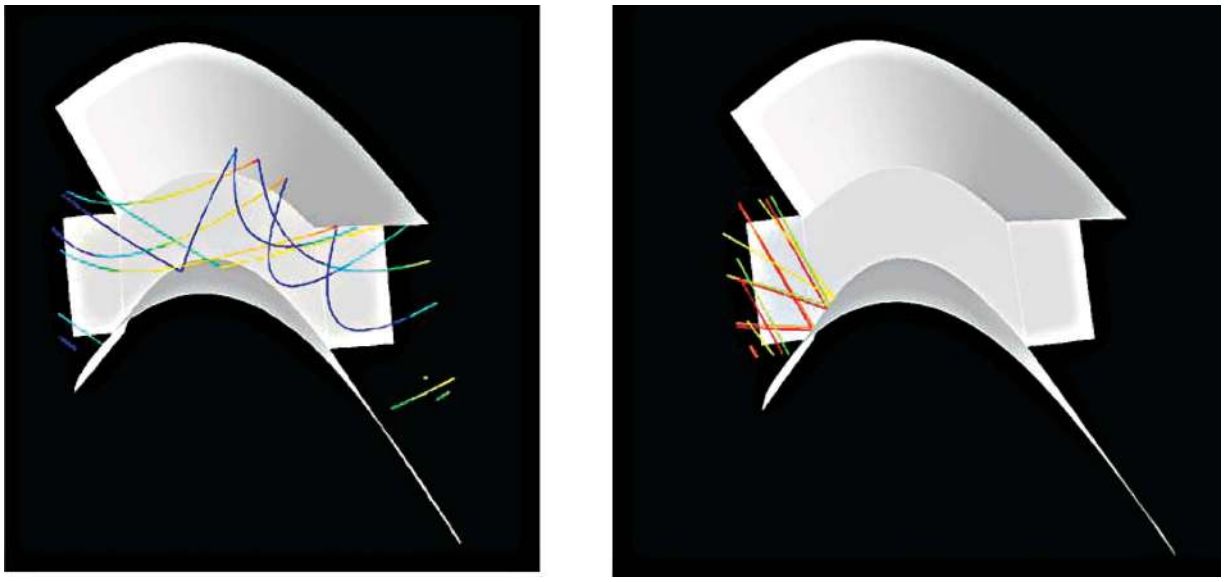

Fig. 11 Top view of particle trajectories through rotor: (a) (left) 30 μm particles and (b) (right) 1500 μm particles

surface impact data to compute the vane erosion rate per unit surface area per unit mass of ingested particles in the turbine. Figure 14 shows increasing erosion rates over the vane's pressure surface toward the trailing edge and a narrow high-erosion band at the vane's leading edge.

Summary

Turbine vane/blade surface deterioration is strongly dependent on the turbine geometry, blade surface material, and particle characteristics. Experimental results for blade and coating material erosion indicate that both erosion rate and surface roughness increase with the eroding particle impact velocities and impingement angles and that larger particles produce higher surface roughness. The computational results of particle dynamics simulations indicate that many particles impact the vane pressure surface and that the larger particles cross over and impact the vane suction surface toward the trailing edge. The vane surface impacts reduce the particles' absolute velocity and, consequently, they impact the rotor blade suction surface. Predictions based on the com-

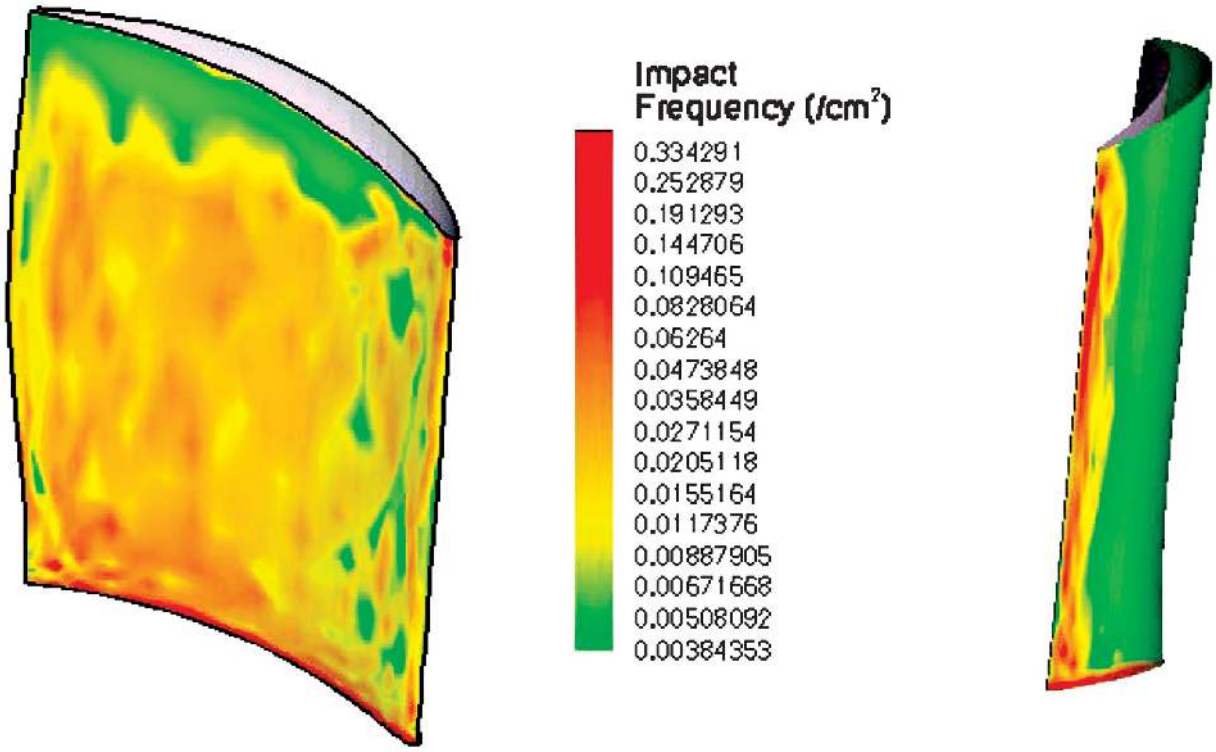

Fig. 12 Impact frequency: (a) (left) vane pressure surface and (b) (right) vane leading edge

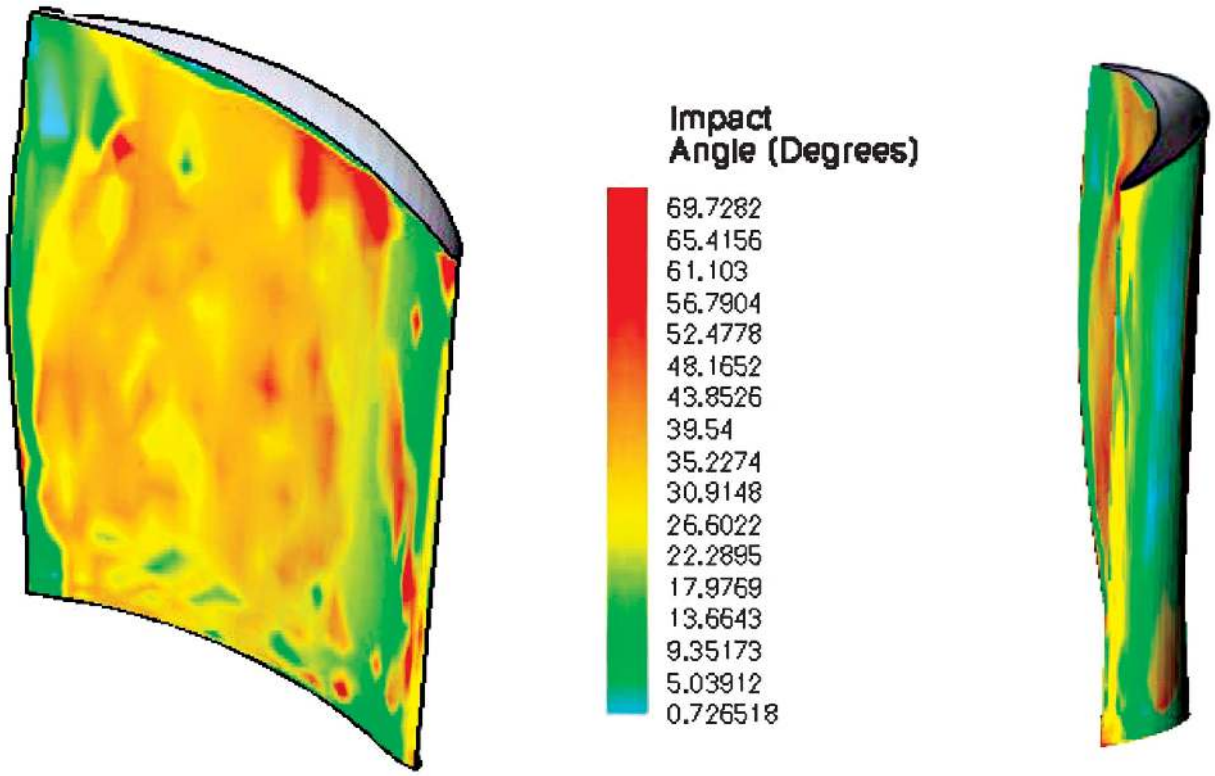

Fig. 13 Particle mean impact angle: (a) (left) vane pressure surface and (b) (right) vane leading edge

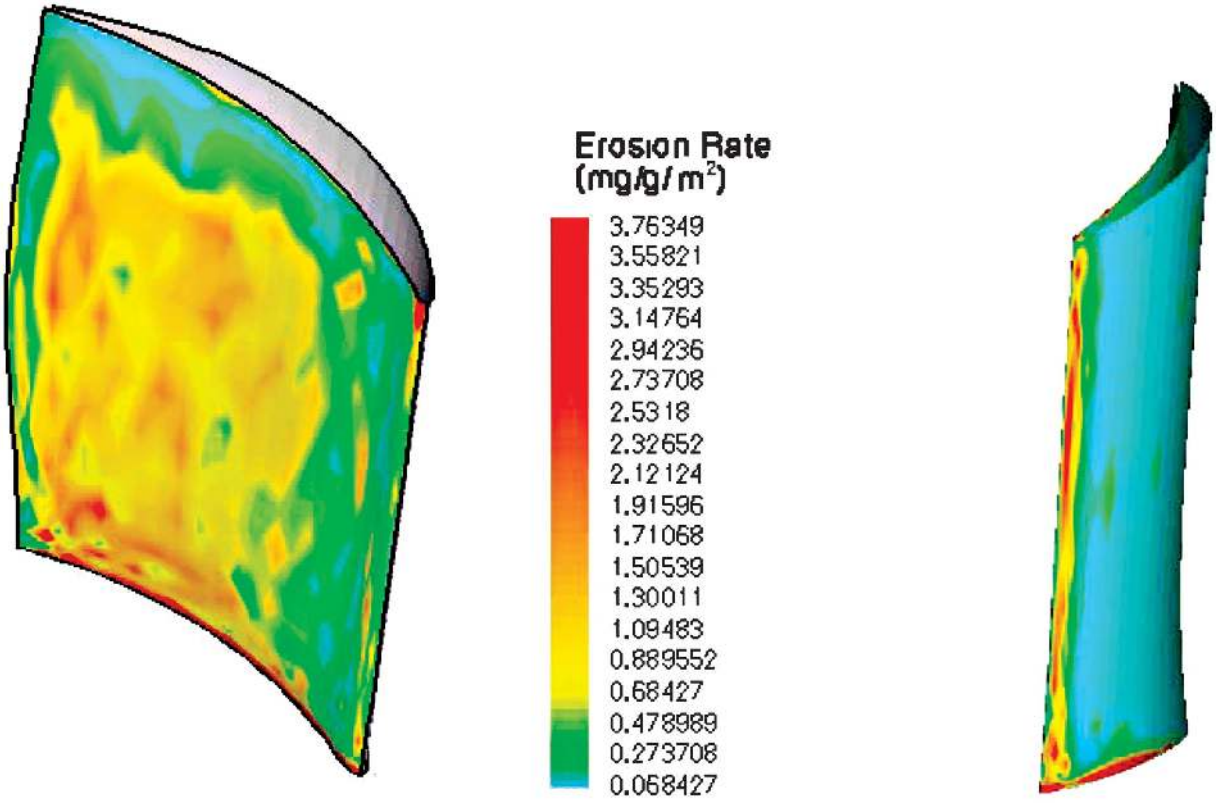

Fig. 14 Erosion Rate: (a) (left) vane pressure surface and (b) (right) vane leading edge

puted particle trajectories and the experimental characterization of coated cane material indicates a narrow band of high erosion at the vane leading edge and pressure surface erosion increasing toward the trailing edge.

Acknowledgment

This work was sponsored by the US Department of Energy through a grant in cooperation with the South Carolina Institute for Energy Studies (UTSR) at Clemson University. Project Monitor: Richard Wenglarz.

Nomenclature

D_p = particle diameter, μm
E = erosion rate (material removal per unit mass of particles)
R = roughness profile from linear 2D surface measurements, μm
S = roughness profile from linear 3D surface measurements, μm
$\bar{u}$ = gas velocity
$\bar{u}_p$ = particle velocity
Re = Reynolds number based on slip velocity $(\bar{u}-\bar{u}_p)$ and particle diameter (D_p)
ρ = density
μ = molecular viscosity
D_q = mean profile slope of the profile elements within a sampling length, deg

Subscripts

a = arithmetic mean deviation of the profile, z units
q = rms deviation of the profile, z units
v = maximum depth of the profile below the mean line of the profile, z units
p = maximum height of the profile above the mean line of the profile, z units
t = maximum peak to valley of the profile, z units
pc = mean height of the elements, z units

References

[1] Hamed, A., and Tabakoff, W., 1994, "Experimental and Numerical Simulation of Ingested Particles in Gas Turbine Engines," *AGARD (NATO) 83rd Symposium of Propulsion and Energetics Panel on Turbines, Rotterdam*, The Netherlands, April 25-28.
[2] Tabakoff, W., 1995, "High-Temperature Erosion Resistance Coatings for Use in Turbomachinery," Wear **186-187**, pp. 224–229.
[3] Tabakoff, W., 1999, "Protection of Coated Superalloys From Erosion in Turbomachinery and Other Systems Exposed to Particulate Flows," Wear **233-235**, pp. 200–208.
[4] Tabakoff, W., Hamed, A., and Wenglarz, R., 1988, "Particulate Flows, Turbomachinery Erosion and Performance Deterioration," Von Karman Lecture Series 1988–1989, May 24–27, Brussels, Belgium.
[5] Balan, C., and Tabakoff, W., 1984, "Axial Flow Compressor Performance Deterioration," AIAA 84-2108.
[6] Hamed, A., Tabakoff, W., and Singh, D., 1998, "Modeling of Compressor Performance Deterioration Due to Erosion," Int. J. Rotating Mach. **4**, pp. 243–248.
[7] Taylor, R. P., 1990, "Surface Roughness Measurements on Gas Turbine Blades," ASME J. Turbomach. **112**, pp. 175–180.
[8] Tarada, F., and Suzuki, M., 1993, "External Heat Transfer Enhancement to Turbine Blading Due to Surface Roughness," *ASME IGTI*, Cincinnati, May, ASME, New York, ASME Paper 93-GT-74.
[9] Bons, J. P., Taylor, R. P., McClain, S. T., and Rivir, R. B., 2001, "The Many Faces of Turbine Surface Roughness," *Proc. of ASME Turbo Expo*, June, New Orleans, ASME, New York, ASME Paper No. 2001-GT-0163.
[10] Blair, M. F., 1994, "An Experimental Study of Heat Transfer in a Large-Scale Turbine Rotor Passage," ASME J. Turbomach. **116**, pp. 1–13.
[11] Hoffs, A., Drost, U., and Bolcs, A., "Heat Transfer Measurements on a Turbine Airfoil at Various Reynolds Numbers and Turbulence Intensities Including Effects of Surface Roughness," *IGTI, Birmingham, UK*, June 1996, ASME, New York, ASME Paper No. 96-GT-169.
[12] Bogard, D. G., Schmidt, D. L., and Tabbita, M., 1998, "Characterization and Laboratory Simulation of Turbine Airfoil Surface Roughness and Associated Heat Transfer," ASME J. Turbomach. **120**, pp. 337–342.
[13] Abuaf, N., Bunker, R. S., and Lee, C. P., 1998, "Effects of Surface Roughness on Heat Transfer and Aerodynamic Performance of Turbine Airfoils," ASME J. Turbomach. **120**, pp. 522–529.
[14] McCay, L., 1973, "The Coal Burning Gas Turbine Project," Report of Interdepartmental Gas Turbine Steering Committee, Australian Government Publishing Service.
[15] Tabakoff, W., Hamed, A., and Metwally, M., 1991, "Effect of Particle Size Distribution on Particle Dynamics and Blade Erosion in Axial Flow Turbines," ASME J. Eng. Gas Turbines Power **113**, pp. 607–615.
[16] Metwally, M., Tabakoff, W., and Hamed, A., 1995, "Blade Erosion in Automotive Gas Turbine Engine," ASME J. Eng. Gas Turbines Power **117**, pp. 213–219.
[17] Hamed, A., and Kuhn, T. P., 1995, "Effects of Variational Particle Restitution Characteristics on Turbomachinery Erosion," ASME J. Eng. Gas Turbines Power **117**, pp. 432–440.
[18] Hamed, A., 1989, "Influence of Secondary Flow on Turbine Erosion," ASME J. Turbomach. **111**(3), pp. 310–314.
[19] Tabakoff, W., Malak, M. F., and Hamed, A., 1987, "Laser Measurements of Solid Particles Rebound Parameters Impinging 2024 Aluminum and 6Al-4V Titanium Alloys," AIAA J. **25**(5), pp. 721–726.
[20] Tabakoff, W., Murugan, D. M., and Hamed, A., 1994, "Effects of Target Materials on the Particle Restitution Characteristics for Turbomachinery Application," AIAA Paper No. 94-0143.
[21] *FLUENT 6.1 User's Guide*, 2003.
[22] Tabakoff, W., Hamed, A., Metwally, M., Yeuan, J., and Pasin, M., 1990, "Study of Particle Rebound Characteristics and Material Erosion at High Temperatures," Final Technical Report, Fossil Energy Materials Program, US Department of Energy, ORNL/Sub/84-89628/03.
[23] Tabakoff, W., Hamed, A., Metwally, M., and Yeuan, J., "Study of Particle Rebound Characteristics and Material Erosion at High Temperatures," ORNL/FMP 902, AR&TD Fossil Energy Materials Semi-Annual Progress Report for Period Ending 09-30-1990, ORNL, Part IV, pp. 381–393.
[24] Morsi, S. A., and Alexander, A. J., 1972, "An Investigation of Particle Trajectories in Two-Phase Flow Systems," J. Fluid Mech., **50**(2), pp. 193–208.
[25] Haider, A., and Levenspiel, O., 1989, "Drag Coefficient and Terminal Velocity of Spherical and Nonspherical Particles," Powder Technol. **58**, pp. 63–70.